

# Physics Opportunities for Vector-Boson Scattering at a Future 100 TeV Hadron Collider

B. Jäger<sup>1</sup>, L. Salfelder<sup>1</sup>, M. Worek<sup>2</sup>, D. Zeppenfeld<sup>3</sup>

<sup>1</sup> *Institute for Theoretical Physics, University of Tübingen, Auf der Morgenstelle 14, 72076 Tübingen, Germany*

<sup>2</sup> *Institut for Theoretical Particle Physics and Cosmology, RWTH Aachen University, 52056 Aachen, Germany*

<sup>3</sup> *Institute for Theoretical Physics, KIT, 76128 Karlsruhe, Germany*

## Abstract

Vector-boson scattering (VBS) processes provide particularly promising means for probing the mechanism of electroweak symmetry breaking and to search for new physics in the weak sector. In the environment of a future proton-proton collider operating at a center-of-mass energy of 100 TeV, unprecedented opportunities arise for the investigation of this important class of reactions. We highlight the prominent features of VBS processes in this energy regime and discuss how the VBS signal can be isolated in the presence of a priori large QCD backgrounds. We find excellent opportunities for the analysis of VBS reactions in a kinematic range that is inaccessible to present colliders.

# 1 Introduction

With the discovery of the Higgs boson at the CERN Large Hadron Collider (LHC) by the ATLAS [1] and CMS collaborations [2] particle physics has entered a new era. However, with the existence of the last missing building block of the Standard Model (SM) being experimentally confirmed, understanding the very mechanism responsible for electroweak symmetry breaking still requires advanced efforts. Complementary to approaches seeking to probe the form of the Higgs potential via measurements of triple and quartic self-interactions of the Higgs boson in processes that are plagued by low event rates and large backgrounds [3–9], weak boson scattering reactions provide promising means to explore the electroweak sector of the SM in an experimentally more easily accessible regime [10–12]. Weak boson scattering processes, i.e. the genuine  $2 \rightarrow 2$  scattering processes  $VV \rightarrow VV$  (with  $V$  denoting a  $W^\pm$  or a  $Z$  gauge boson), are particularly sensitive to new physics in the electroweak gauge boson sector. For instance, in the absence of a light Higgs boson, the amplitudes for the scattering of the longitudinal gauge boson modes,  $V_L V_L \rightarrow V_L V_L$ , would grow unphysically with energy, giving rise to unitarity violations in the TeV regime. Alternatively, new resonances in the weak sector, such as a  $Z'$  boson, could result in prominent peaks in the invariant mass of the final-state  $VV$  system. Since so far no explicit deviations of the SM have been observed experimentally in the weak sector, one expects new physics effects either to be very strongly suppressed or to become visible only in energy regimes that have not been accessible experimentally so far.

At hadron colliders, weak vector-boson scattering (VBS) processes are probed via the scattering of quarks or anti-quarks by the exchange of weak bosons in the  $t$ -channel followed by subsequent emission of weak bosons, i.e. purely electroweak reactions of the type  $qq \rightarrow qqVV$ . The weak gauge bosons in turn decay, either leptonically or hadronically. Because of the color-singlet nature of the weak-boson exchange in these reactions, VBS processes exhibit particularly distinctive features in the detector, the scattered quarks giving rise to two tagging jets in the forward and backward regions, while the decay products of the weak bosons are located in the central-rapidity region. A fairly small scattering angle of those very energetic tagging jets is reflected in their large invariant mass and rather moderate transverse momenta. These characteristics are essential in distinguishing the signal of interest from a priori very large contributions of QCD-induced background processes. Strategies for optimizing signal-to-background ratios for VBS processes at the LHC have been explored in detail, resulting in the first observation of a VBS signal in the  $W^+W^+jj$  mode by the ATLAS [13] and CMS collaborations [14] at a center-of-mass energy of  $\sqrt{s} = 8$  TeV. While only very loose exclusion bounds on new physics effects in the weak sector could be placed with the limited event rates accessible at 8 TeV, stronger bounds are expected from data taken at the higher energy of 13 TeV in LHC Run II.

Much more powerful means for probing VBS processes would be provided, however, by a future high-energy hadron collider operating at an energy of 100 TeV, such as a Future Circular Collider (FCC) currently discussed as a follow-up project of the CERN LHC, or a Chinese Super proton-proton Collider (SppC)<sup>1</sup>. In order to explore the physics capabilities

---

<sup>1</sup>In the following, for simplicity we will use the acronym FCC to generically refer to proton-proton colliders operating at an energy of 100 TeV.

of such a machine, in [15] we have performed a preliminary study of VBS processes in the presence of background reactions at the FCC. A related analysis was performed in Ref. [16]. Here, we go beyond that work and present a detailed signal-background analysis for VBS processes taking into account the following production modes:  $W^+W^+jj$ ,  $W^+Zjj$ ,  $W^+W^-jj$ , and  $ZZjj$ . In all cases leptonic decays of both gauge bosons are considered. Moreover, spin correlations of the decay products, finite width as well as off-shell effects of gauge bosons in the signal and background processes are fully included.

The paper is organized as follows: The general setup of our analysis is described in Sec. 2. A generic way for the parameterization of new physics effects as provided by an effective field theory expansion is presented in Sec. 3. In Sec. 4 for each mode we devise a set of customized cuts to optimize the signal in the presence of QCD-induced  $VVjj$  backgrounds. In the case of  $pp \rightarrow W^+W^-jj$  production, in addition to the QCD induced  $pp \rightarrow W^+W^-jj$  process contributions from the overwhelming  $t\bar{t}$  background processes are considered. Here additional techniques are applied to suppress this background in order to improve the signal-to-background ratio. Our conclusions are presented in Sec. 5.

## 2 Setup of the analysis

Throughout this analysis, for each  $pp \rightarrow VVjj$  VBS process and its associated QCD backgrounds we focus on a particular decay mode with a clean experimental signature. We assume that each weak boson  $V$  decays leptonically and we consider decays of the  $VV$  systems only into two different generations of leptons. For instance, for the VBS-induced  $W^+W^+jj$  production mode we consider the  $\nu_e e^+ \nu_\mu \mu^+ jj$  final state at  $\mathcal{O}(\alpha^6)$ . Other lepton combinations in the final state (such as  $\nu_e e^+ \nu_e e^+$  and  $\nu_\mu \mu^+ \nu_\mu \mu^+$ ) can be obtained thereof straightforwardly, as long as same-type lepton interference effects are neglected. These interference effects are completely negligible, in particular in the kinematic range we are interested in, with large invariant masses of the four-lepton system that disfavor same-type lepton interference configurations. The cross section summed over different lepton flavors ( $\ell = e, \mu$ ) can be obtained by multiplying the result for a single leptonic flavor channel with a suitable combinatorial factor. Off-shell and non-resonant contributions of the gauge bosons are fully taken into account. For simplicity, we nonetheless refer to the respective process as “ $VVjj$  production”, implicitly assuming that decays of the weak bosons are taken into account. Identical-flavor interference effects between  $t$ - and  $u$ -channel diagrams are neglected for all signal processes. Triple gauge-boson production processes of the type  $pp \rightarrow VVV$  with subsequent decay of a weak boson into a pair of jets are assumed to be part of a different reaction and not considered here. Even though such processes in principle give rise to the same final state as VBS processes, they exhibit entirely different kinematic properties and can be safely neglected after the application of VBS specific selection cuts. The Cabibbo-Kobayashi-Maskawa (CKM) mixing of the quark generations is neglected, i.e. a diagonal form is assumed for the CKM matrix, since mixing within the first two generations cancels exactly within the  $t$ -channel approximation as no charm tagging is attempted. For all  $VVjj$  processes, contributions from external top or bottom quarks are regarded as separate processes not to be considered here.

For the QCD background processes all Feynman diagrams that result in the specified

final state at  $\mathcal{O}(\alpha_s^2\alpha^4)$  are accounted for with all interference effects as well as non-zero gauge boson width effects. We shall refer to these processes as “ $VVjj$  QCD production”. In the same way we proceed for background processes with top-quarks. We consider  $t\bar{t}$ ,  $t\bar{t}j$  and  $t\bar{t}jj$  production, respectively, at  $\mathcal{O}(\alpha_s^2\alpha^4)$ ,  $\mathcal{O}(\alpha_s^3\alpha^4)$ ,  $\mathcal{O}(\alpha_s^4\alpha^4)$ . We include all double-, single- and non-resonant diagrams, interference effects as well as off-shell effects of the top quarks. Additionally, non-resonant and off-shell effects due to the finite  $W$ -boson width are taken into account. We always combine these three background processes into the “ $t\bar{t} + \text{jets}$ ” sample. We note here that for all top-quark processes massive final-state bottom quarks will be considered. Calculations for all signal and background processes are performed at the leading order (LO).

The numerical simulations that form the basis of our discussion below make use of the VBFNLO package [17] for the VBS signal processes. All background processes are computed with the HELAC-DIPOLES package [18] and cross-checked with the HELAC-PHEGAS Monte-Carlo program [19]. Both the HELAC-DIPOLES and HELAC-PHEGAS programs use for the calculation of scattering amplitudes an automatic off-shell iterative algorithm [20–22]. For the phase-space integration, PHEGAS [23] in conjunction with PARNI [24] as well as KALEU [25] have been employed.

In order to warrant the correctness of our results we have cross-checked HELAC-DIPOLES results with VBFNLO for all processes that are implemented in the VBFNLO program. In each case we found full agreement for cross sections and distributions within the numerical accuracy of the two codes.

Throughout, for the masses  $m$  and widths  $\Gamma$  of the  $W$ ,  $Z$ , and  $H$  bosons we use the following values:

$$\begin{aligned} m_W &= 80.385 \text{ GeV}, & \Gamma_W &= 2.097547 \text{ GeV}, \\ m_Z &= 91.1876 \text{ GeV}, & \Gamma_Z &= 2.508827 \text{ GeV}, \\ m_H &= 125.09 \text{ GeV}, & \Gamma_H &= 0.004066 \text{ GeV}. \end{aligned} \tag{1}$$

Further electroweak (EW) parameters such as the EW coupling  $\alpha$  and the weak mixing angle  $\sin\theta_W$  are computed in the  $G_\mu$  scheme with the Fermi constant  $G_F = 1.1663787 \times 10^{-5} \text{ GeV}^{-2}$ . The mass and width of the top quark are set to

$$m_{top} = 172.5 \text{ GeV}, \quad \Gamma_{top} = 1.4576 \text{ GeV}. \tag{2}$$

For the parton distribution functions (PDFs) of the proton, we use the MMHT2014lo68cl set [26] for all electroweak and QCD-induced  $VVjj$  processes. For  $t\bar{t} + \text{jets}$  production the MMHT2014lo68cl\_nf4 PDF set is used instead. Consequently, in the former case we use the so called five-flavor-scheme, whereas, in the latter we employed the so-called four-flavor scheme with only gluons and light-flavor quarks in the proton, where massive bottom quarks are produced from gluon splitting at short distances. The mass of the bottom quark is set to

$$m_b = 4.75 \text{ GeV}. \tag{3}$$

The associated strong coupling  $\alpha_s$  running at one loop is provided by the LHAPDF repository [27].

The factorization and renormalization scales,  $\mu_F$  and  $\mu_R$ , are set process-specifically: The VBS signal processes  $pp \rightarrow VVjj$  with fully leptonic decays are of the order of

$\mathcal{O}(\alpha^6)$ . The leading order VBS results are, thus, independent of  $\mu_R$ . For  $\mu_F$ , we use the momentum transfer  $Q_i$  of the incoming to the outgoing (anti-)quark on the upper and lower fermion lines, respectively,

$$\mu_F = Q_i. \quad (4)$$

For the QCD-induced  $VVjj$  production processes, which are of the order of  $\mathcal{O}(\alpha_s^2\alpha^4)$ , the total transverse energy  $H_T^{VV}$  of each event is used as reference scale, such that

$$\mu_F = \mu_R = H_T^{VV}/2, \quad (5)$$

with

$$H_T^{VV} = \sum_i p_{T,i} + E_T(V_1) + E_T(V_2). \quad (6)$$

Here, the summation runs over the transverse momenta  $p_{T,i}$  of all final-state partons involved in an event, while the transverse energy of each gauge boson is computed from its mass and the momenta of its leptonic decay products according to

$$E_T(V_i) = \sqrt{p_T^2(V_i) + m_{V_i}^2}, \quad (7)$$

where  $i$  denotes a  $W^\pm$  or  $Z$  boson. Similarly, for the top-quark induced background processes, that are respectively of the order of  $\mathcal{O}(\alpha_s^2\alpha^4)$ ,  $\mathcal{O}(\alpha_s^3\alpha^4)$  and  $\mathcal{O}(\alpha_s^4\alpha^4)$ , we use

$$\mu_F = \mu_R = H_T^{\text{top}}/2, \quad (8)$$

with the transverse energy  $H_T^{\text{top}}$  being computed from the transverse energy of the top quarks or anti-quarks,

$$E_T(t) = \sqrt{p_T^2(t) + m_{top}^2}, \quad E_T(\bar{t}) = \sqrt{p_T^2(\bar{t}) + m_{top}^2}. \quad (9)$$

and the transverse momenta of all light partons in the final state of an event,

$$H_T^{\text{top}} = \sum_i p_{T,i} + E_T(t) + E_T(\bar{t}). \quad (10)$$

In the following sections we will derive dedicated selection cuts for each VBS process. However, a common set of minimal selection cuts will be applied in each case: In order to reconstruct jets from partons, we use the anti- $k_T$  jet algorithm [28] with  $R = 0.4$ . We require at least two jets. The two hardest jets of each event are called ‘‘tagging jets’’ and need to have a minimum transverse momentum of

$$p_{T,\text{jet}} \geq 50 \text{ GeV}. \quad (11)$$

The two tagging jets are also required to reside in opposite hemispheres of the detector,

$$y_{j_1}^{\text{tag}} \times y_{j_2}^{\text{tag}} < 0. \quad (12)$$

Charged leptons need to fulfill cuts on transverse momenta, rapidities, and be well separated from any jet in the rapidity-azimuthal angle plane,

$$p_{T,\ell} \geq 20 \text{ GeV}, \quad |y_\ell| \leq 5, \quad \Delta R_{\text{jet},\ell} \geq 0.4. \quad (13)$$

A very powerful tool for the suppression of background processes is provided by requiring that all charged leptons are located between the two tagging jets in rapidity

$$y_{j,min}^{\text{tag}} < y_\ell < y_{j,max}^{\text{tag}}. \quad (14)$$

To suppress contributions from virtual photons,  $\gamma^* \rightarrow \ell^+\ell^-$ , we furthermore impose the minimal invariant-mass cut on oppositely charged (same flavor) leptons, that occur in both  $ZZjj$  and  $W^\pm Zjj$  processes. Thus, in these channels we require

$$M_{e^+e^-} > 15 \text{ GeV}, \quad M_{\mu^+\mu^-} > 15 \text{ GeV}. \quad (15)$$

### 3 Effective field theory expansion

A generic way for the parameterization of new physics effects is provided by an effective field theory (EFT) expansion. Such an effective theory can be constructed as a low-energy approximation of a more fundamental theory, and it is valid only up to a specific energy scale  $\Lambda$ . The Lagrangian of an EFT is typically expressed in terms of the SM Lagrangian and additional terms including operators  $\mathcal{O}_i^{(d)}$  of higher dimensionality  $d$ ,

$$\mathcal{L}_{\text{EFT}} = \mathcal{L}_{\text{SM}} + \sum_{d>4} \sum_i \frac{f_i^{(d)}}{\Lambda^{d-4}} \mathcal{O}_i^{(d)}, \quad (16)$$

with  $f_i^{(d)}$  denoting the coefficients of the expansion. As long as an energy regime far below the breakdown scale  $\Lambda$  of the EFT expansion is considered, the non-SM part of the EFT expansion is dominated by the lowest relevant terms, i.e. contributions due to operators of dimension six and eight.

Since dimension-six operators affect quartic as well as triple gauge boson couplings, they can most conveniently be probed in gauge-boson pair production processes that exhibit the respective triple-gauge boson vertices. The dimension-eight operators below, instead, do not have any impact on triple but only on quartic gauge boson couplings that emerge in triple-vector boson production and VBS reactions. The experimentally clean VBS processes thus represent a particularly important test bed for this class of new-physics contributions (see, e.g. Ref. [29] for a recent review). In the present study, we therefore consider the impact of new physics on VBS processes in the EFT approach that is due to CP conserving operators of dimension eight that modify quartic weak gauge boson couplings. Following the notation of Refs. [30–32], we consider a set of representative dimension-eight operators,  $\mathcal{O}_i^{(d=8)}$ , which in the literature are referred to as  $\mathcal{O}_{S,1}$ ,  $\mathcal{O}_{M,1}$ , and  $\mathcal{O}_{T,0}$ , respectively. They are defined as

$$\mathcal{O}_{S,1} = [(D_\mu \Phi)^\dagger (D^\mu \Phi)] \times [(D_\nu \Phi)^\dagger (D^\nu \Phi)], \quad (17)$$

$$\mathcal{O}_{M,1} = \text{Tr} [\hat{W}_{\mu\nu} \hat{W}^{\nu\beta}] \times [(D_\beta \Phi)^\dagger (D^\mu \Phi)], \quad (18)$$

$$\mathcal{O}_{T,0} = \text{Tr} [\hat{W}_{\mu\nu} \hat{W}^{\mu\nu}] \times \text{Tr} [\hat{W}_{\alpha\beta} \hat{W}^{\alpha\beta}], \quad (19)$$

with the associated coefficients  $f_{S,1}/\Lambda^4$ ,  $f_{M,1}/\Lambda^4$ , and  $f_{T,0}/\Lambda^4$ . To simplify the notation we drop the dimensionality index ( $d = 8$ ) here and in the following. The considered

operators contain the Higgs-doublet field  $\Phi$ , the covariant derivative  $D_\mu$ , and the field-strength tensor  $W_{\mu\nu}$ , defined as

$$D_\mu = \partial_\mu + \frac{i}{2}g\tau^I W_\mu^I + \frac{i}{2}g'B_\mu, \quad (20)$$

$$W_{\mu\nu} = \frac{i}{2}g\tau^I(\partial_\mu W_\nu^I - \partial_\nu W_\mu^I - g\epsilon_{IJK}W_\mu^J W_\nu^K), \quad (21)$$

with the U(1) and SU(2) gauge fields  $B_\mu$  and  $W_\mu$ , the associated couplings  $g'$  and  $g$ , the weak isospin matrices  $\tau^I$ , and

$$\hat{W}_{\mu\nu} = i\frac{g}{2}W_{\mu\nu}^a\sigma^a. \quad (22)$$

By construction, the EFT approach is valid only in a restricted energy regime. If the EFT expansion is truncated, unphysical violations of unitarity may occur beyond some scale  $\Lambda_U$ . Such unitarity violations can be avoided, if the EFT is restricted to the region where it is fully valid. Practically, this can be achieved by form factors that suppress EFT contributions above scales where the EFT expansion is supposed to lose its applicability. In the code package VBFNLO the impact of dimension-six and dimension-eight operators on VBS processes is explicitly accounted for. The user can set the relevant operator coefficients to customized values. In order to maintain unitarity, a form factor

$$F = \begin{cases} 1 & \dots & M_{VV} < \Lambda_F \\ \left(\frac{\Lambda_F}{M_{VV}}\right)^4 & \dots & M_{VV} > \Lambda_F \end{cases} \quad (23)$$

can be applied, where  $M_{VV}$  denotes the invariant mass of the produced  $V$  bosons in  $VVjj$  reactions. Note that  $\Lambda_F \leq \Lambda_U$ , and  $\Lambda_F$  is related to  $\Lambda$ , but not necessarily identical.

## 4 Signal and background processes

In order to fully exploit the capabilities of a future 100 TeV proton-proton collider for the analysis of VBS processes, optimized selection cuts for each specific final state need to be devised. In the following, we present process-specific selection criteria for various VBS channels and discuss the behavior of signal and background contributions for characteristic kinematic distributions.

### 4.1 $W^+W^+jj$

The same-sign diboson-plus-dijet final state,  $pp \rightarrow W^+W^+jj$ , provides a particularly clean signature in the fully leptonic decay mode, as the only irreducible background in the  $\nu_e e^+ \nu_\mu \mu^+ jj$  channel comprises the QCD-induced  $W^+W^+jj$  production process. In contrast to other VBS channels that receive large background contributions from gluon-induced QCD processes, same-sign diboson production can only proceed via the scattering of (anti-)quarks of proper type to ensure the conservation of electromagnetic charge throughout the reaction. In the next-to-leading-order QCD analysis of [33] it was shown that with VBS-specific selection cuts a signal-to-background ( $S/B$ ) ratio of about 27 could be achieved at the LHC operating at an energy of 7 TeV. This ratio seems remarkable at

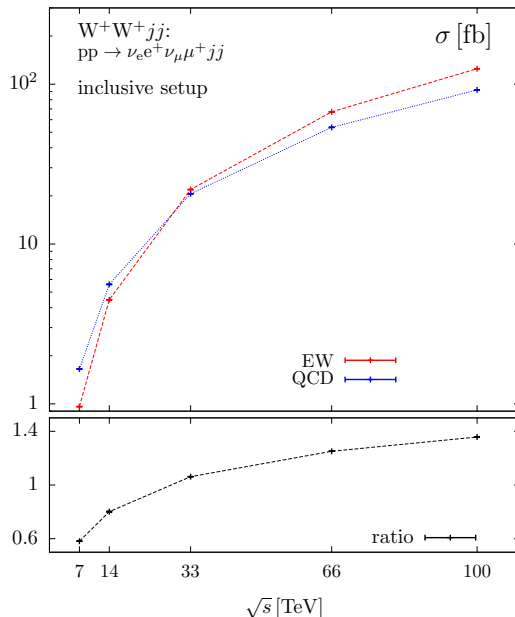


Figure 1: Energy dependence of the EW-induced (red line) and QCD-induced (blue line) contributions to the inclusive cross section for  $pp \rightarrow \nu_e e^+ \nu_\mu \mu^+ jj$ , without any selection cuts. The lower panel shows the ratio of the EW to the QCD contribution.

first sight, if one naively assumes the size of the respective EW and QCD cross sections to be determined by the relevant orders of the strong and electromagnetic couplings that themselves differ by roughly one order of magnitude. Upon closer inspection it becomes clear that the *inclusive* cross section for the QCD-induced  $\nu_e e^+ \nu_\mu \mu^+ jj$  final state indeed exceeds the EW one by about a factor of 1.7. However, the very distinct kinematic properties of the VBS production mode allow the efficient suppression of the QCD background contributions with a dedicated set of selection cuts that diminish the rate of signal events only marginally, resulting in the large  $S/B$  ratio reported above. At higher collider energies, the production rate for the EW signal process increases slightly faster than the production rate for the QCD background, as depicted in Fig. 1. We will see below that an approach similar to the strategy applied at the 7 TeV LHC can be used for higher center-of-mass energies yielding even better  $S/B$  ratios at a 100 TeV collider.

To illustrate the capability of selection cuts in the environment of an FCC, focusing on a fully inclusive setup (i.e. not imposing any selection cuts) in Fig. 2 we present two distributions that exhibit particularly distinctive shapes in VBS-induced processes: the invariant mass  $M_{jj}$  of the tagging jets' system and the rapidity separation of the two tagging jets,  $\Delta y_{jj}$ . While in QCD-induced  $W^+W^+jj$  processes the two jets are mostly produced with a small invariant mass and close to each other in rapidity, the color-singlet nature of the weak-boson exchange, which is characteristic for VBS processes, gives rise to a dijet system of large invariant mass with a substantial separation in rapidity. This feature can be exploited for the design of powerful selection cuts. It can be easily seen from Fig. 2 that the  $\Delta y_{jj}$  distribution (right panel) peaks around zero values for the QCD background, while the VBS contribution exhibits a dip there, and peaks around



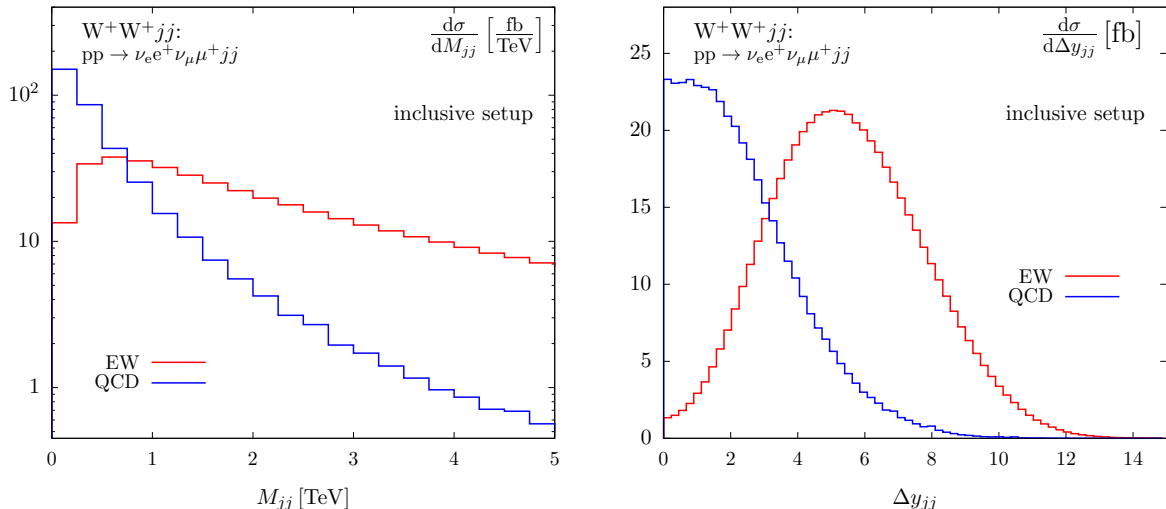


Figure 2: *Invariant mass (l.h.s.) and rapidity separation of the two tagging jets (r.h.s) for the EW-induced (red lines) and QCD-induced (blue lines) contributions to  $pp \rightarrow \nu_e e^+ \nu_\mu \mu^+ jj$ , without any selection cuts.*

$\Delta y_{jj} = 5$ . On the other hand, a steep rise of the invariant mass distribution towards small values of  $M_{jj}$  can be observed in case of the QCD induced  $W^+W^+jj$  production process, where the VBS contribution is no longer dominant. Suitable cuts on  $M_{jj}$  and  $\Delta y_{jj}$  diminish the signal cross section only marginally, at the same time removing a large fraction of the QCD-induced background contribution. Indeed, by imposing the following process-specific selection cuts,

$$M_{jj} > 500 \text{ GeV}, \quad \Delta y_{jj} = |y_{j_1} - y_{j_2}| > 1.5, \quad (24)$$

in addition to the generic cuts of Eqs. (11)–(14) we obtain cross sections of  $\sigma_S = 49.34$  fb for the signal process and  $\sigma_B = 1.68$  fb for the background process, resulting in the  $S/B$  ratio of about 30, similar to what was reported in [33] for the case of the LHC operating at 7 TeV. Figure 3 shows the invariant mass and rapidity separation of the tagging jet system within the selection cuts of Eqs. (11)–(14) and Eq. (24).

New physics in the weak sector is expected to affect not only the shape of distributions related to the weak bosons in  $VVjj$  processes, but also differential distributions of the tagging jets that are the tell-tale signature of VBS reactions at hadron colliders. In particular the tails of invariant-mass and transverse-momentum distributions of final-state leptons and tagging jets are sensitive to physics beyond the SM (BSM). At the FCC, such observables are accessible up to much higher scales than at the LHC. Our study in [15] revealed, for instance, that even at scales far above 1 TeV, several signal events are to be expected for an integrated luminosity of  $30 \text{ fb}^{-1}$ . In the  $W^+W^+jj$  channel, after VBS-specific selection cuts are applied the QCD background contributions amount to only about 3% of the EW signal and thus have little impact on the relevant distributions, as we demonstrate explicitly for selected observables: Figure 4 shows the transverse-momentum and the rapidity distributions of the hardest tagging jet, while

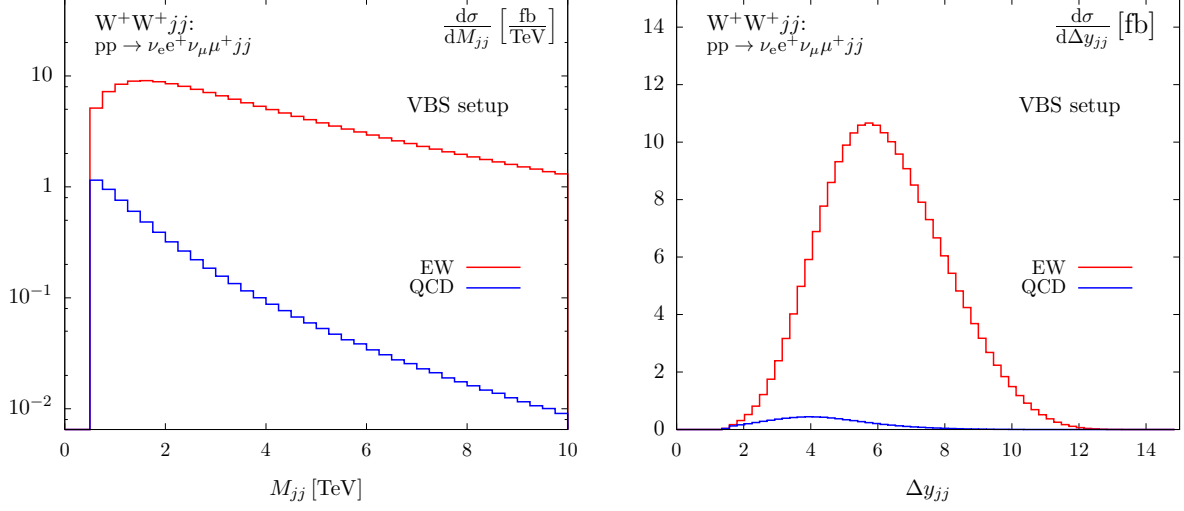


Figure 3: Invariant mass (l.h.s.) and rapidity separation of the two tagging jets (r.h.s) for the EW-induced (red lines) and QCD-induced (blue lines) contributions to  $pp \rightarrow \nu_e e^+ \nu_\mu \mu^+ jj$ , within the selection cuts of Eqs. (11)–(14) and Eq. (24).

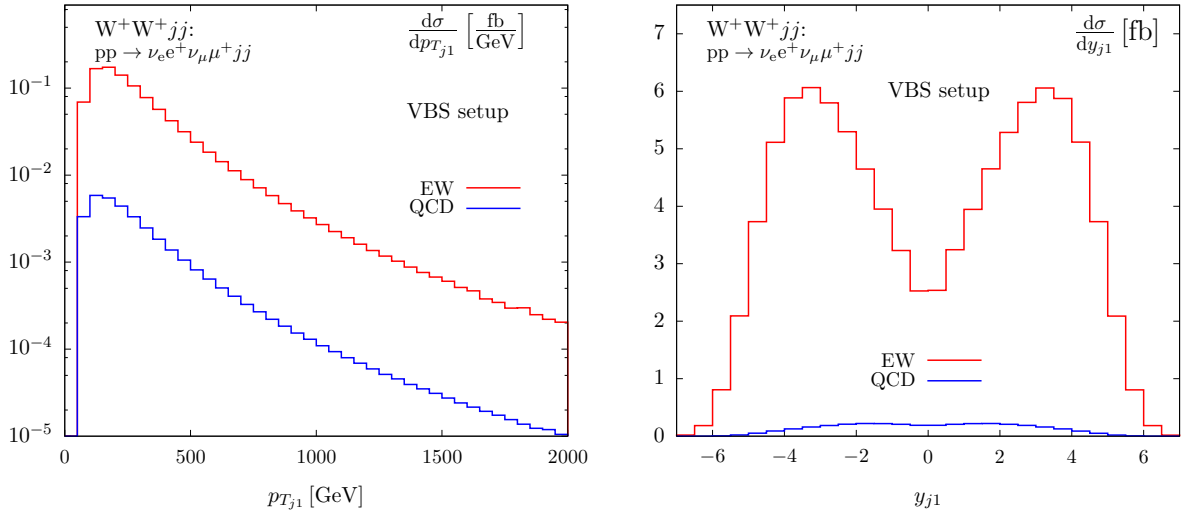


Figure 4: Transverse-momentum (l.h.s.) and rapidity distribution of the hardest tagging jet (r.h.s) for the EW-induced (red lines) and QCD-induced (blue lines) contributions to  $pp \rightarrow \nu_e e^+ \nu_\mu \mu^+ jj$ , within the selection cuts of Eqs. (11)–(14) and Eq. (24).

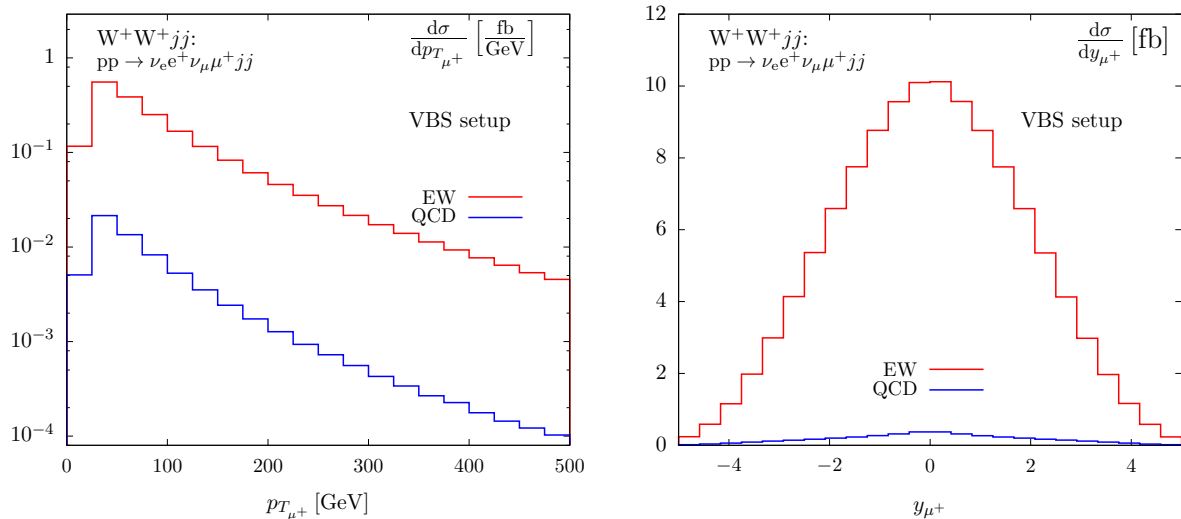


Figure 5: *Transverse-momentum (l.h.s.) and rapidity distribution of the muon (r.h.s) for the EW-induced (red lines) and QCD-induced (blue lines) contributions to  $pp \rightarrow \nu_e e^+ \nu_\mu \mu^+ jj$ , within the selection cuts of Eqs. (11)–(14) and Eq. (24).*

Fig. 5 illustrates the respective distributions of the muon. The transverse-momentum distribution of the hardest tagging jet in the EW signal process exhibits a peak at about 170 GeV, while the QCD contribution tends to produce slightly softer jets. The tagging jets produced in the QCD mode typically are located at smaller rapidities than in the EW signal process where peaks in  $d\sigma/dy_{j_1}$  occur at values as large as  $\pm 4$ . The muon distributions are less distinctive, as the leptons are mostly located at central rapidities in both production modes.

For narrowing down new physics searches in the weak sector, it may be useful to consider a particular mass range of the invariant diboson system. In the  $\nu_e e^+ \nu_\mu \mu^+ jj$  channel, however, the invariant mass of the  $W^+W^+$  system is not fully reconstructible experimentally, because of the presence of two neutrinos. In this case, the transverse mass  $M_{T_{WW}}$  of the final state system consisting of two charged leptons and missing transverse momentum in the detector, can be considered instead. It is defined as

$$M_{T_{WW}} = \sqrt{(E_T^{\ell\ell} + E_T^{miss})^2 - (\vec{p}_T^{\ell\ell} + \vec{p}_T^{miss})^2}, \quad (25)$$

with

$$E_T^{\ell\ell} = \sqrt{(\vec{p}_T^{\ell\ell})^2 + M_{\ell\ell}^2}, \quad E_T^{miss} = |\vec{p}_T^{miss}|. \quad (26)$$

where,  $\vec{p}_T^{\ell\ell}$  denotes the transverse momentum of the charged-lepton system, and  $\vec{p}_T^{miss}$  is the total transverse momentum of the neutrino system. The missing transverse momentum is shown together with the transverse-mass distribution of the lepton-neutrino system for  $pp \rightarrow \nu_e e^+ \nu_\mu \mu^+ jj$  in Fig. 6 in the context of the SM. The latter distribution is particularly interesting to study the applicability of an EFT approach for estimating the impact of new physics in the weak sector.

Figure 7 shows  $d\sigma/dM_{T_{WW}}$  for the EW signal process, both in the context of the SM

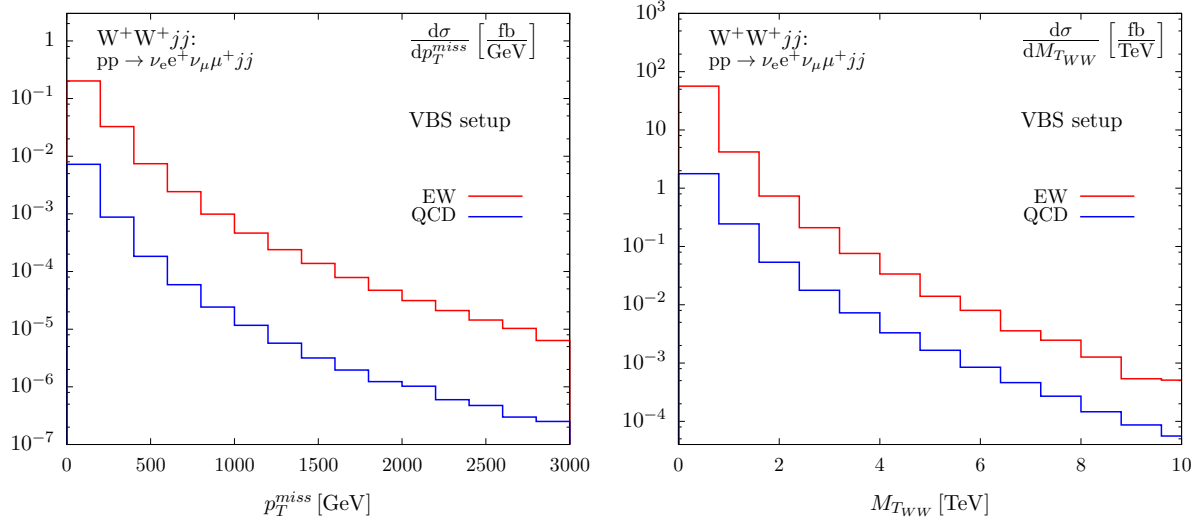


Figure 6: *Missing transverse momentum (l.h.s.) and transverse-mass distribution of the gauge-boson system (r.h.s) for the EW-induced (red lines) and QCD-induced (blue lines) contributions to  $pp \rightarrow \nu_e e^+ \nu_\mu \mu^+ jj$ , within the selection cuts of Eqs. (11)–(14) and Eq. (24).*

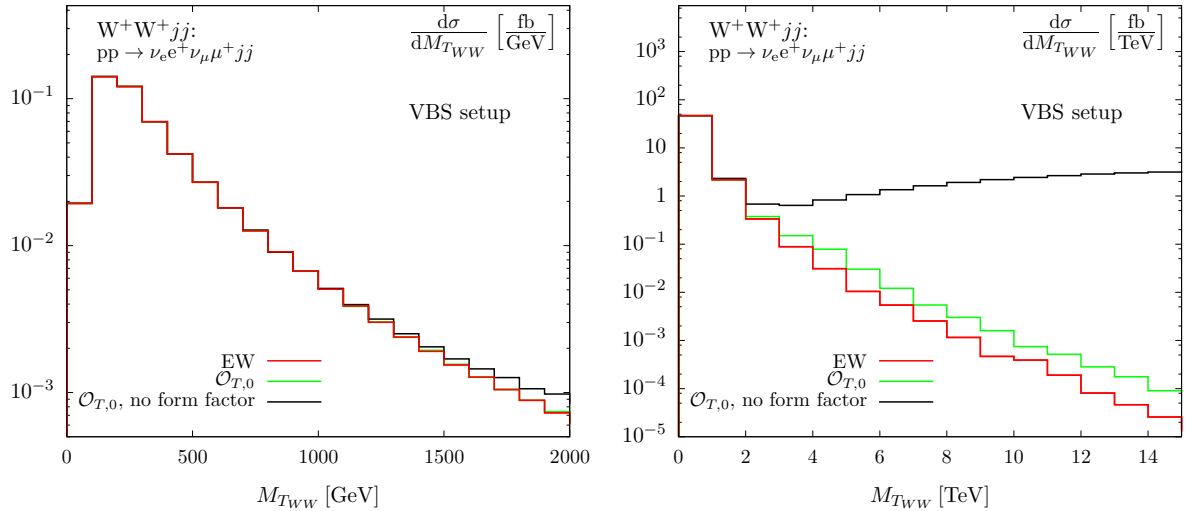


Figure 7: *Transverse-mass distribution of the gauge-boson system for the process  $pp \rightarrow \nu_e e^+ \nu_\mu \mu^+ jj$  in the framework of the SM (red lines) and including the impact of the dimension-eight operator  $\mathcal{O}_{T,0}$  without (black lines) and with (green lines) the form factor of Eq. (23), in two different plot ranges. The selection cuts of Eqs. (11)–(14) and Eq. (24) are imposed.*

and with an additional dimension-eight operator contribution following the EFT expansion of Eq. (16). In particular, we set the coefficient  $f_{T,0}/\Lambda^4 = 0.1/\text{TeV}^4$ , while all other non-SM contributions are assumed to vanish. New-physics contributions characterized by a coefficient of that size would not give rise to experimentally detectable signatures at the 13 TeV LHC. It is thus particularly interesting to see which impact they have on observables at a 100 TeV FCC.

As expected, deviations from the SM mostly occur at high scales. At scales far above  $M_{T_{WW}} \sim 2$  TeV, a naive implementation of contributions from dimension-eight operators gives rise to an unphysical rise of the distribution. This behavior can be avoided by a form factor suppressing contributions beyond the reach of validity of the EFT expansion. Requiring the VBS cross sections to preserve unitarity at all scales, a suppression factor of the form specified in Eq. (23) with the scale  $\Lambda_F = 4.7$  TeV provides sufficient damping. The actual value of this scale factor has been obtained with the help of the calculator [34] available from [35].

The impact of other dimension-eight operators on the transverse-mass distribution of the gauge-boson system is less pronounced. To enhance their relative impact on observables, we impose an additional transverse-mass cut of

$$M_{T_{WW}} > 2 \text{ TeV} . \quad (27)$$

Such a cut reduces the VBS cross section from  $\sigma_{\text{SM}} = 49.34$  fb in the framework of the SM and  $\sigma_{T,0} = 49.52$  fb with the additional EFT contribution of the  $\mathcal{O}_{T,0}$  operator with the coefficient and form factor suppression given above to  $\sigma_{\text{SM}}^{\text{cut}} = 0.48$  fb and  $\sigma_{T,0}^{\text{cut}} = 0.66$  fb, respectively. Obviously, the application of a severe cut on the gauge-boson system significantly improves the relative impact of the EFT contribution on the VBS cross section, although clearly the event rate at such high transverse-mass scales is small such that considerable integrated luminosity will be required to achieve a significant signature.

In Fig. 8 the transverse-mass and missing transverse-momentum distributions for our default  $W^+W^+jj$  settings with the additional cut of Eq. (27) are shown separately for the SM and for simulations where either of the representative operator contributions  $\mathcal{O}_{S,1}$ ,  $\mathcal{O}_{M,1}$ , or  $\mathcal{O}_{T,0}$  has been taken into account. In each case, the respective coefficient  $f_{S,1}/\Lambda^4$ ,  $f_{M,1}/\Lambda^4$ , or  $f_{T,0}/\Lambda^4$  has been set to  $0.1/\text{TeV}^4$ , with all other EFT coefficients set to zero. To avoid unphysical unitarity violations at high energies, we apply form factors using the functional form of Eq. (23) with  $\Lambda_F = 4.3$  TeV for the  $\mathcal{O}_{S,1}$  operator,  $\Lambda_F = 8.3$  TeV for  $\mathcal{O}_{M,1}$ , and – as above –  $\Lambda_F = 4.7$  TeV for  $\mathcal{O}_{T,0}$ . The values of all scale factors have been fixed with the help of [34].

Clearly, a non-vanishing contribution from the  $\mathcal{O}_{T,0}$  operator has the largest impact on each distribution. The operator  $\mathcal{O}_{M,1}$  gives rise to slight enhancements in the tails of both considered distributions, while the impact of the  $\mathcal{O}_{S,1}$  operator is barely distinguishable from the SM prediction. In the following, we will only consider contributions of the  $\mathcal{O}_{T,0}$  operator.

We note that the application of the transverse-mass cut of Eq. (27) in addition to the  $W^+W^+jj$  specific selection cuts of Eqs. (11)–(14) and Eq. (24) changes the cross section contributions of the EW and QCD production modes in the framework of the SM from the values without such a cut to  $\sigma_{\text{EW}}^{\text{cut}} = 0.48$  fb and  $\sigma_{\text{QCD}}^{\text{cut}} = 0.04$  fb. The large transverse mass goes hand-in-hand with an even larger invariant mass of the  $W^+W^+$  system, which

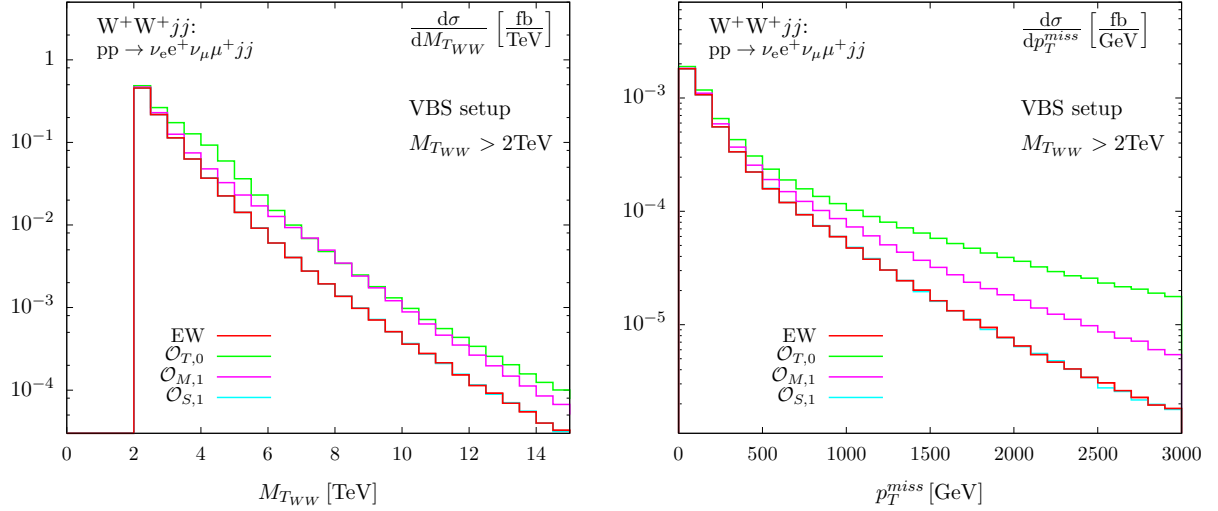


Figure 8: *Transverse-mass (l.h.s.) and missing transverse momentum distributions (r.h.s) for the process  $pp \rightarrow \nu_e e^+ \nu_\mu \mu^+ jj$  in the framework of the SM (red lines) and including the impact of the dimension-eight operators  $\mathcal{O}_{S,1}$  (cyan lines),  $\mathcal{O}_{M,1}$  (magenta lines), and  $\mathcal{O}_{T,0}$  (green lines) supplied by an appropriate form factor. The selection cuts of Eqs. (11)–(14), Eq. (24), and the additional transverse-mass cut of Eq. (27) are imposed.*

requires more energetic incoming quarks, on average. This induces a higher invariant mass of the tagging jet pair and, since the jet  $p_T$ 's remain of the order  $m_W$ , the tagging jets also are found at somewhat larger rapidity. This is illustrated for the rapidity distribution of the hardest jet and the rapidity separation of the two tagging jets in Fig. 9, which are to be compared to the respective distributions without the  $M_{T_{WW}}$  cut, shown in Figs. 4 and 3. The slightly higher tagging jet rapidities are also reflected in a larger rapidity separation of the two tagging jets which now peaks around  $\Delta y_{jj} \approx 8$  for the EW mode (as compared to about 6.5 before the transverse-mass cut). A similar trend of larger rapidities occurs for the QCD background. Since the event rates associated with the QCD production mode are very small, however, this does not pose a serious issue for the separation of signal and background in this high-invariant mass regime. Note that excellent forward rapidity coverage of the hadron calorimeters is needed at the FCC in order not to lose a substantial fraction of VBS events in this particularly interesting region of high invariant mass of the vector boson pair.

## 4.2 $W^+ Z jj$

In contrast to the  $W^+ W^+ jj$  channel that is free of gluon-induced background processes, all other VBS reactions are plagued by large QCD backgrounds that require more powerful cuts on the tagging-jets system than those that have been considered in the  $W^+ W^+ jj$  mode.

To quantify this statement, let us consider the representative  $pp \rightarrow e^+ \nu_e \mu^+ \mu^- jj$  final state for the  $W^+ Z jj$  channel. With the basic cuts of Eqs. (11)–(15), the associated

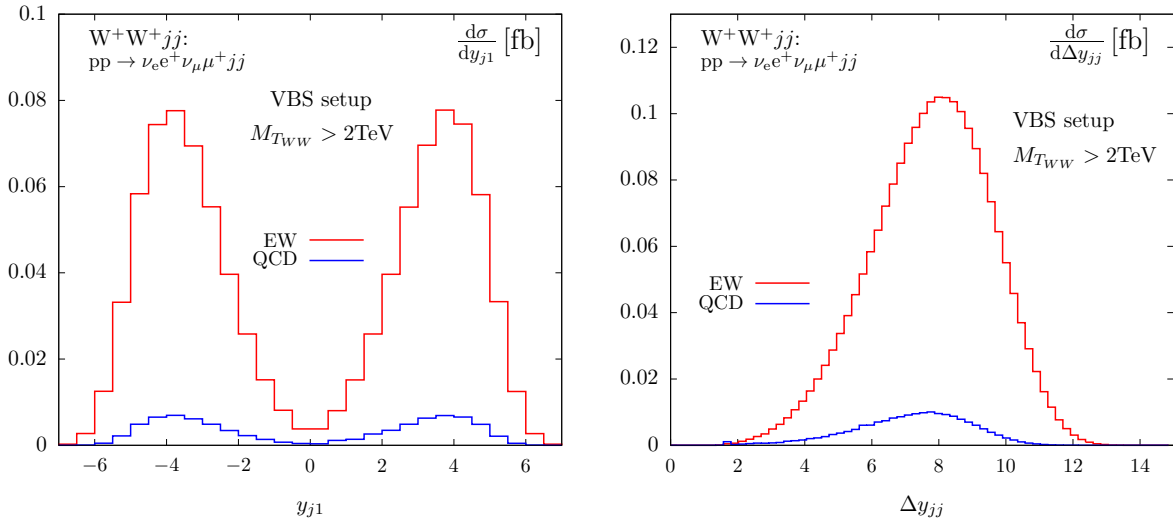


Figure 9: Rapidity distribution of the hardest tagging jet (l.h.s) and rapidity separation of the two tagging jets (r.h.s) for the EW-induced (red lines) and QCD-induced (blue lines) contributions to  $pp \rightarrow \nu_e e^+ \nu_\mu \mu^+ jj$ , within the selection cuts of Eqs. (11)–(14), (24), and the additional transverse-mass cut of Eq. (27).

QCD background cross section,  $\sigma_{\text{basic}}^{\text{QCD}} = 23.38$  fb, by far overshoots the EW signal cross section,  $\sigma_{\text{basic}}^{\text{EW}} = 8.46$  fb, resulting in a  $S/B$  ratio of less than 0.4. Besides the basic cuts of Eqs. (11)–(15) severe additional cuts on the tagging jets' invariant mass and rapidity separation need to be applied to significantly reduce the impact of the QCD background. In particular, we require

$$M_{jj} > 2500 \text{ GeV}, \quad \Delta y_{jj} > 5. \quad (28)$$

Indeed, with these customized selection cuts, the VBS cross section is reduced by merely about 40% with respect to the value obtained with basic selection cuts only, while the QCD cross section goes down by a factor of 8.4. As a consequence, one arrives at signal and background cross sections of, respectively,  $\sigma_S = 5.08$  fb and  $\sigma_B = 2.79$  fb, resulting in a  $S/B$  ratio of about 1.8.

Figure 10 illustrates clearly the different behavior of the dijet system in the  $W^+Zjj$  mode compared to the  $W^+W^+jj$  channel considered in Figure 3. While in the  $W^+W^+jj$  channel the VBS contribution exceeds the QCD contribution in the entire plotted range of  $M_{jj}$ , in the  $W^+Zjj$  mode this is the case only in the tail of the distribution. Already at around  $M_{jj} \sim 3.5$  TeV the QCD contribution starts to dominate and steeply rises towards smaller values of the invariant mass. Even though the  $pp \rightarrow e^+ \nu_e \mu^+ \mu^- jj$  final state contains a neutrino that is invisible to the detector, the invariant-mass distribution of the leptonic decay products,  $M_{WZ}$ , can be reconstructed, if kinematic constraints are used to determine the longitudinal component of the neutrino momentum. In the framework of the SM, there exists no particle with appropriate quantum numbers and mass to resonantly produce an on-shell  $W^+Z$  system. The invariant-mass distribution thus does not exhibit pronounced resonance peaks, but is characterized by a broad continuum, as

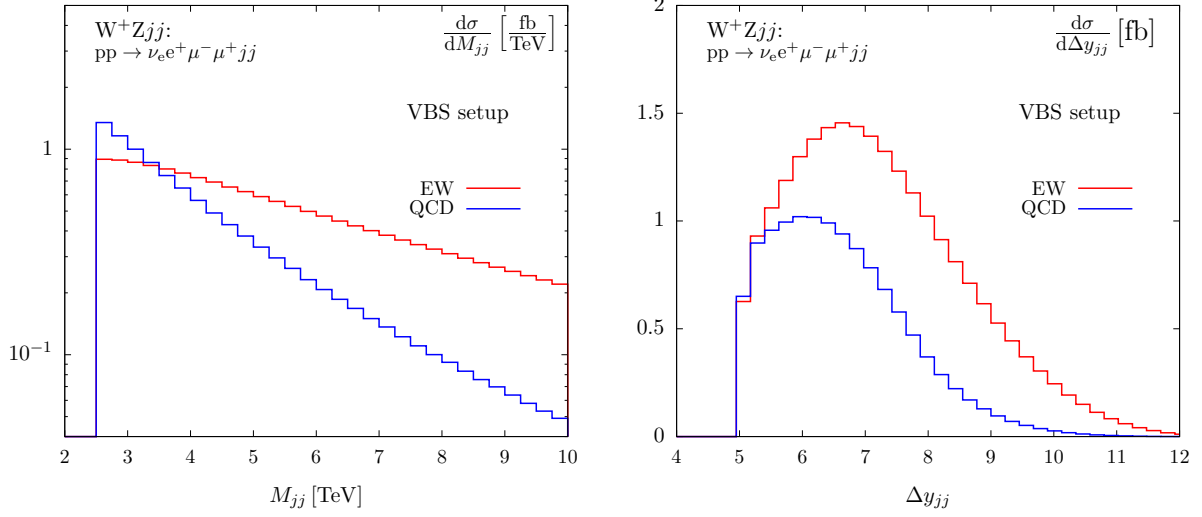


Figure 10: *Invariant mass (l.h.s.) and rapidity separation of the two tagging jets (r.h.s) for the EW-induced (red lines) and QCD-induced (blue lines) contributions to  $pp \rightarrow \nu_e e^+ \mu^- \mu^+ jj$ , within the selection cuts of Eqs. (11)–(15) and Eq. (28).*

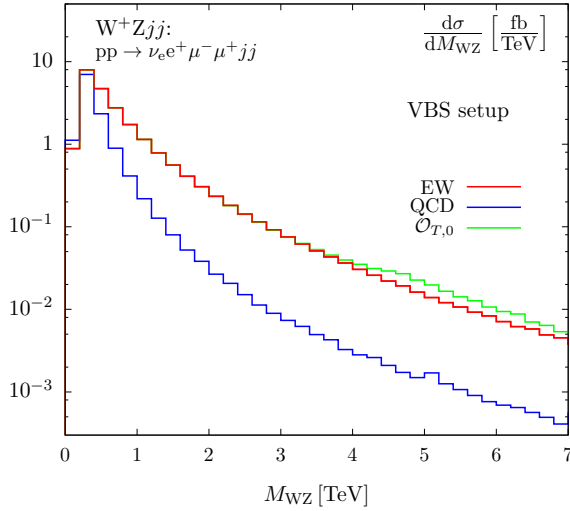


Figure 11: *Invariant-mass distribution of the  $WZ$  system reconstructed from the lepton momenta for the process  $pp \rightarrow \nu_e e^+ \mu^- \mu^+ jj$ . Shown are the QCD-induced contributions (blue line), and the EW-induced contributions in the framework of the SM (red line) and including the impact of the dimension-eight operator  $\mathcal{O}_{T,0}$  (green line) with the form factor of Eq. (23). The selection cuts of Eqs. (11)–(15) and Eq. (28) are applied.*



can be observed in Fig. 11 in the framework of the SM and with an additional dimension-eight operator contribution following the EFT expansion of Eq. (16). To simulate the latter, we set the coefficient  $f_{T,0}/\Lambda^4 = 0.1/\text{TeV}^4$  and supply a suppression factor of the form specified in Eq. (23) with the scale  $\Lambda_F = 4.7 \text{ TeV}$ . All other non-SM contributions are assumed to vanish. Above  $M_{WZ} = 4 \text{ TeV}$  one finds  $\sigma_{\text{SM}}^{\text{cut}} = 0.047 \text{ fb}$  for the SM and  $\sigma_{T_0}^{\text{cut}} = 0.061 \text{ fb}$  in the presence of the  $T_0$  coupling. With sufficient integrated luminosity the difference will be highly significant.

Distinct peaks in the  $M_{WZ}$  spectrum are expected in BSM models featuring new particles that can resonantly decay into the  $WZ$  system. The most prominent examples comprise models with a  $W'$  boson or Kaluza-Klein models where the compactification of an extra space-time dimension gives rise to a tower of new gauge bosons with masses larger than a few hundred GeV. The impact of such new resonances on VBS signatures, in the context of the LHC, was discussed for example in [36].

### 4.3 $ZZjj$

Compared to VBS processes involving  $W$  bosons, relatively small event rates are encountered for  $ZZjj$  VBS production, in particular in the fully leptonic decay modes. This is partly due to the fact that the electroweak couplings of  $Z$  bosons to quarks that occur in the associated VBS production process are smaller than respective couplings involving  $W$  bosons. Moreover, the branching ratios of the  $Z$  bosons to charged leptons are approximately three times smaller than the branching ratios of the  $W$  bosons into  $\ell\nu$  pairs. Nonetheless,  $ZZjj$  reactions provide a very clean testbed for VBS processes since the kinematics of the  $ZZ$  system is fully reconstructible, if final states with four charged leptons are considered. We will thus focus on the  $pp \rightarrow e^-e^+\mu^-\mu^+jj$  process in the following. We note that, although we simplistically refer to the process under consideration as  $ZZjj$  production, QCD and EW production of  $e^-e^+\mu^-\mu^+jj$  final states include also Feynman diagrams with the exchange of photons instead of  $Z$ -bosons, and respective interference contributions. These diagrams fully have to be taken into account for the computation of meaningful cross sections, in order not to violate electroweak gauge invariance. Potentially divergent contributions involving a  $\gamma^* \rightarrow \ell^+\ell^-$  splitting at very low photon virtuality are removed, however, by the invariant-mass cuts of Eq. (15). In order to suppress contributions from QCD-induced  $e^-e^+\mu^-\mu^+jj$  production, we require

$$M_{jj} > 2000 \text{ GeV}, \quad \Delta y_{jj} > 3, \quad (29)$$

in addition to the basic cuts of Eqs. (11)–(15). With these cuts we have obtained the cross sections  $\sigma_S = 2.18 \text{ fb}$  and  $\sigma_B = 0.23 \text{ fb}$  for the signal and background processes, respectively, resulting in the S/B ratio of almost 10.

For the EW signal process the invariant-mass distribution of the four-lepton system,  $d\sigma/dM_{ZZ}$ , exhibits a rich resonance structure, featuring peaks at  $m_{4\ell} = M_{ZZ} = m_Z$ , and at the Higgs resonance  $M_{ZZ} \approx m_H$ , as can be seen in Fig. 12. Similar to the  $W^+W^+jj$  channel discussed before, we explore the impact of the dimension-eight operator  $\mathcal{O}_{T,0}$  on the  $ZZjj$  reaction, setting the EFT coefficient  $f_{T,0}/\Lambda^4 = 0.1/\text{TeV}^4$ , and assuming all other non-SM contributions to be negligible. To warrant unitarity conservation up to the highest scales, we use the form factor of Eq. (23) with  $\Lambda_F = 4.7 \text{ TeV}$ . For the VBS cross

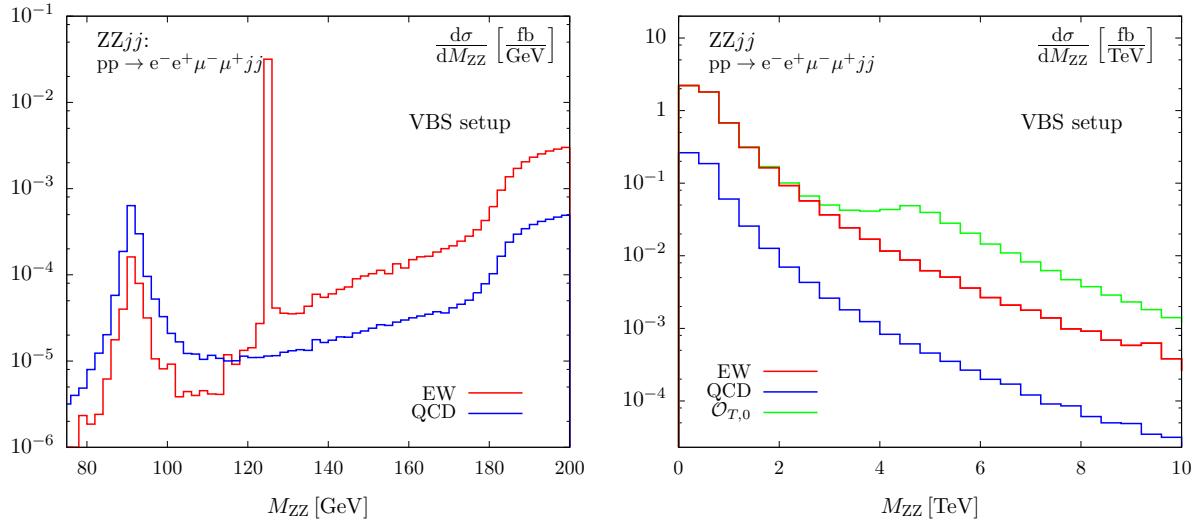


Figure 12: *Invariant-mass distribution of the  $ZZ$  system reconstructed from the lepton momenta in two different plot ranges for the process  $pp \rightarrow e^-e^+\mu^-\mu^+jj$  in the framework of the SM (red and blue lines) and including the impact of the dimension-eight operator  $\mathcal{O}_{T,0}$  (green line) with the form factor of Eq. (23). The selection cuts of Eqs. (11)–(15) and Eq. (29) are imposed.*

section in the context of the SM and the respective EFT result within the  $ZZjj$ -specific selection cuts of Eqs. (11)–(15) and Eq. (29), we find results that are rather similar to each other,  $\sigma_{SM} = 2.18$  fb and  $\sigma_{EFT} = 2.30$  fb. As becomes obvious from an inspection of the invariant mass distribution in the TeV range, shown in the right panel of Fig. 12, differences between the SM and the EFT prediction are most pronounced at high scales. Indeed, by applying an additional selection cut of

$$M_{ZZ} > 2 \text{ TeV}, \quad (30)$$

the relative difference between the VBS cross section in the context of the SM and the respective EFT result can be significantly enhanced, yielding  $\sigma_{SM}^{\text{cut}} = 0.11$  fb and  $\sigma_{EFT}^{\text{cut}} = 0.22$  fb, i.e. even anomalous couplings substantially smaller than  $0.1 \text{ TeV}^{-4}$  can be seen in this channel with  $3000 \text{ fb}^{-1}$ . Note that in the high-invariant mass region most sensitive to the EFT operator the impact of the QCD-induced background is negligible.

#### 4.4 $W^+W^-jj$

The  $W^+W^-jj$  mode exhibits the largest cross section of all VBS channels. Nonetheless, extracting the VBS signal from the background is particularly challenging in this mode, because in addition to the QCD-induced  $W^+W^-jj$  contribution very large background rates arise from top-quark pair production processes. First, in reactions of the type  $pp \rightarrow t\bar{t}$ , almost all top quarks decay into  $W$  bosons and bottom quarks. The bottom quarks may be misidentified experimentally as light-flavor tagging jets. Together with the decay products of the  $W$  bosons, such bottom-jets may give rise to signatures very similar to the

VBS signal process. Second, the light jets occurring in  $t\bar{t} + \text{jets}$  production processes may mimic the tag jets characteristic of VBS reactions. Because of the large production rates associated with these top-quark induced production processes, they remain a significant source of background even after the application of stringent selection cuts.

For our analysis, we focus on the  $e^+\nu_e\mu^-\bar{\nu}_\mu jj$  final state. In addition to the QCD-induced  $pp \rightarrow e^+\nu_e\mu^-\bar{\nu}_\mu jj$  background, we consider the top-quark pair production process,  $pp \rightarrow e^+\nu_e\mu^-\bar{\nu}_\mu b\bar{b}$ , together with the associated production of a top-quark pair with one and two jets, i.e.  $pp \rightarrow e^+\nu_e\mu^-\bar{\nu}_\mu b\bar{b}j$  and  $pp \rightarrow e^+\nu_e\mu^-\bar{\nu}_\mu b\bar{b}jj$ , where  $j$  stands for a light quark or a gluon. All top-quark induced background processes are simulated with the HELAC-DIPOLES package where all double-, single and non-resonant contributions, interferences and off-shell effects due to the finite width of the top quarks and  $W$  bosons are fully incorporated in the matrix element calculations. In case of the top-quark pair production process both massive bottom quarks from top-quark decays are identified as the tagging jets. We will denote this process as  $t\bar{t}$  production. In case of the  $e^+\nu_e\mu^-\bar{\nu}_\mu b\bar{b}j$  and  $e^+\nu_e\mu^-\bar{\nu}_\mu b\bar{b}jj$  processes various phase-space regions can be studied. First, for  $e^+\nu_e\mu^-\bar{\nu}_\mu b\bar{b}j$  we can identify the phase-space region where both bottom quarks are again associated with the two (hardest) tagging jets whereas an additional light quark or gluon is not restricted by any cuts. This configuration is, however, properly described only by next-to-leading-order calculations like the one described, for example, in Ref. [37]. Since we are interested in LO results only we do not consider higher order corrections to the  $t\bar{t}$  production process and discard this configuration. Nevertheless, there is still another distinctly different region of phase space, which can be studied at LO, namely the one where the final state light quark or gluon can give rise to one tagging jet, and one of the two bottom jets is identified as the other tagging jet. We shall call this configuration  $t\bar{t}j$  production. In the next step, we consider  $e^+\nu_e\mu^-\bar{\nu}_\mu b\bar{b}jj$  production. Once more we can identify two massive bottom quarks as the two tagging jets and leave additional partons unrestricted. This is, however, a next-to-next-to-leading-order correction to  $t\bar{t}$  production. We can also identify only one bottom quark with one tagging jet and the second tagging jet with a light quark or gluon. This is, however, a part of the next-to-leading-order corrections to our  $t\bar{t}j$  production process, where results from Ref. [38,39] could be of help. We disregard these cases and keep only the new configuration where the final state light quarks or gluons are the two tagging jets and both bottom quarks are unconstrained. We denote this part of the top-quark background as  $t\bar{t}jj$ . In each case two tagging jets are subject to the cuts of Eqs. (11)–(14).

Discrimination between jets originating from  $b$ -quarks and those emerging from light quarks or gluons can be very helpful to further suppress  $t\bar{t} + \text{jets}$  backgrounds in the  $W^+W^-jj$  channel. The top-induced background contributions can be suppressed most efficiently by removing all events that contain an identified bottom jet. To this end a  $b$ -tagging jet veto is applied to eliminate any events where at least one of the tagging jets is identified as arising from a  $b$ -quark or anti-quark. The procedure can be applied to both the  $t\bar{t}$  and  $t\bar{t}j$  production processes. However, the  $b$ -tagging efficiency is not ideal. Since we are not aware of a respective study for future 100 TeV  $pp$  colliders we concentrate on related results for the LHC to estimate the impact of the  $b$ -jet tagging efficiency on the  $b$ -tagging jet veto. To this end we incorporate the CMS analysis of Ref. [40] for our assumptions on  $b$ -tagging efficiencies and mis-tagging probabilities. To be more precise,

$p_{T,\text{jet}}$ [GeV]	$1.4 <  y_j $	$ y_j  < 1.4$
50 - 80	65%	75%
80 - 120	70%	80%
120 - 170	70%	80%
> 170	65%	75%

Table 1: Assumed  $b$ -tagging efficiencies as functions of the transverse momentum of the jet for different rapidity ranges (adapted from [36]).

we assume that the  $b$ -tagging efficiency depends on the transverse momentum and rapidity of the respective tagging jet as detailed in Tab. 1. To diminish the top-quark background even further one can make use of the so-called central-jet veto. For the  $t\bar{t}j$  and  $t\bar{t}jj$  backgrounds one or both of the  $b$ -quarks are not identified as the tagging jets. They will most frequently lie between the two tagging jets in rapidity, i.e. in the region where we look for the decay products of two gauge bosons. Vetoing events with these additional  $b$  jets provides a powerful suppression tool to control the top-quark background. Thus, we reject all events where a  $b$  jet with  $p_{T,b} > 50$  GeV is observed in the rapidity gap region between the two tagging jets,

$$y_{j,\min}^{\text{tag}} < y_{\text{jet}} < y_{j,\max}^{\text{tag}}. \quad (31)$$

We note that extra jet activity does not require a bottom jet, but merely the rejection of any events with an additional jet. In our leading-order simulation, with leptonic decays of both gauge bosons, this central-jet veto criterion only affects the  $t\bar{t}j$  and  $t\bar{t}jj$  backgrounds. At this perturbative order, the  $t\bar{t}$  production process, the QCD-induced and the VBS-type  $W^+W^-jj$  contributions exhibit at most two hard jets that serve as tagging jets. However, additional jet activity would occur also in these reactions in higher-order calculations that include further parton-emission contributions. Moreover, hadronic decays of one or both gauge bosons would contribute to the multiple production of jets in these processes. It is a well-known feature of VBS processes, however, that in contrast to the case of QCD-induced reactions extra parton emission typically occurs close to or more forward than the tagging jets and thus gives rise to little jet activity in the central-rapidity region [41–45]. In addition to the basic cuts of Eqs. (11)–(14), the  $b$ -tagging jet veto as well as the central-jet-veto of Eq. (31), the process-specific cuts of

$$M_{jj} > 2000 \text{ GeV}, \quad \Delta y_{jj} > 5, \quad (32)$$

are used. The cross sections obtained in this way can be summarized as follows:  $\sigma_S = 58.27$  fb,  $\sigma_B^{\text{QCD}} = 22.26$  fb and  $\sigma_B^{t\bar{t}+jets} = 589$  fb ( $\sigma_B^{t\bar{t}} = 0.1528$  fb,  $\sigma_B^{t\bar{t}j} = 84.24$  fb and  $\sigma_B^{t\bar{t}jj} = 505$  fb). These numbers yield a  $S/B$  ratio of 0.09, which obviously would make an extraction of the signal very difficult. To improve the signal to background ratio we

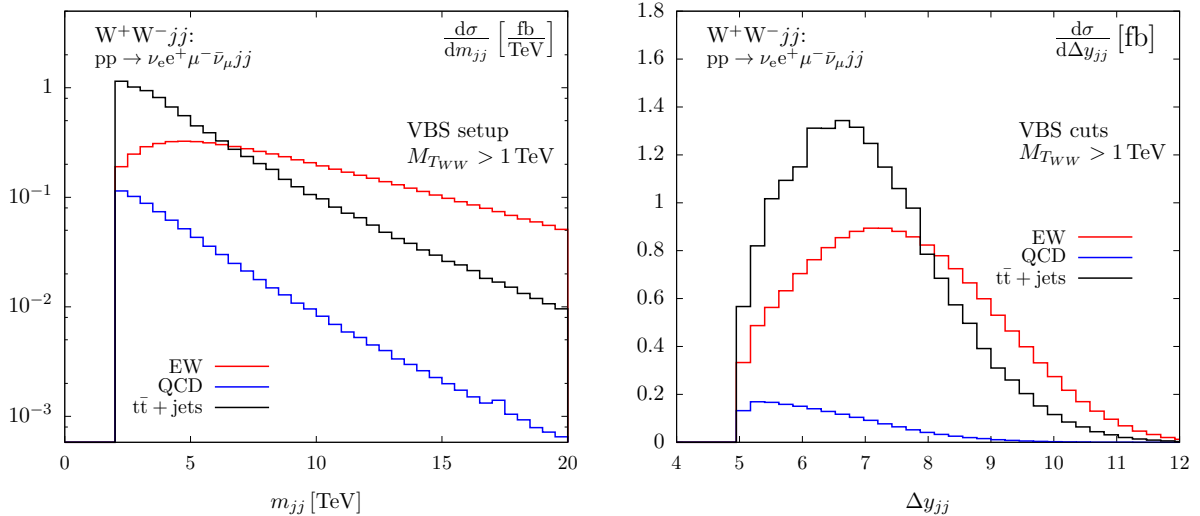


Figure 13: Invariant mass (*l.h.s.*) and rapidity separation (*r.h.s.*) of the tagging jets for the EW-induced signal (red lines), the QCD-induced (blue lines), and the top-quark induced (black lines) background contributions to  $pp \rightarrow e^+ \nu_e \mu^- \bar{\nu}_\mu jj$ , within the selection cuts of Eqs. (11)–(14) and Eqs. (31)–(33).

have thus applied an additional cut on the transverse mass of the final state system reconstructed from the momenta of the charged leptons and the missing transverse momentum due to the neutrinos in the final state according to the definition of Eq. (25),

$$M_{T_{WW}} > 1 \text{ TeV}. \quad (33)$$

With this cut the following cross section results have been obtained instead:  $\sigma_S = 3.59 \text{ fb}$ ,  $\sigma_B^{\text{QCD}} = 0.389 \text{ fb}$  and  $\sigma_B^{\text{tt+jets}} = 4.23 \text{ fb}$  ( $\sigma_B^{\text{tt}} = 0.02 \text{ fb}$ ,  $\sigma_B^{\text{ttj}} = 0.76 \text{ fb}$  and  $\sigma_B^{\text{ttjj}} = 3.45 \text{ fb}$ ). This time the more advantageous  $S/B$  ratio of 0.8 has been reached.

In order to investigate the impact of the  $p_{T,b}$  cut in the central-jet veto procedure on the  $\sigma_B^{\text{ttj}}$  and  $\sigma_B^{\text{ttjj}}$  cross sections, we have relaxed its value to  $p_{T,b} > 100 \text{ GeV}$  once the  $M_{T_{WW}}$  cut has already been applied. With  $p_{T,b} > 100 \text{ GeV}$  we have obtained the following results:  $\sigma_B^{\text{ttj}} = 1.05 \text{ fb}$  and  $\sigma_B^{\text{ttjj}} = 7.61 \text{ fb}$ , that together with  $\sigma_B^{\text{tt}} = 0.02 \text{ fb}$  result in the following total cross section for the top quark background process:  $\sigma_B^{\text{tt+jets}} = 8.68 \text{ fb}$ . A difference by a factor of two with respect to the corresponding result in the setup with a more severe transverse-momentum cut can be observed – the consequence of which is the now less advantageous  $S/B$  ratio of 0.4. Thus, our final setup for the  $W^+W^-jj$  channel comprises the original (harder) central jet-veto cut of  $p_{T,b} > 50 \text{ GeV}$  as well as the set of selection cuts from Eqs. (11)–(14), Eqs. (31)–(33).

Within this setup, Fig. 13 illustrates the invariant-mass and rapidity distributions of the tagging jets. The signal cross section dominates at high invariant mass, decreasing more slowly than the various background contributions. In the rapidity-separation variable, the VBS signal tends to larger values than the top backgrounds and, in particular, the QCD-induced  $W^+W^-jj$  contributions. Together with the transverse-mass cut of Eq. (33) the cuts of Eq. (32) have removed large parts of the QCD- and top-quark-

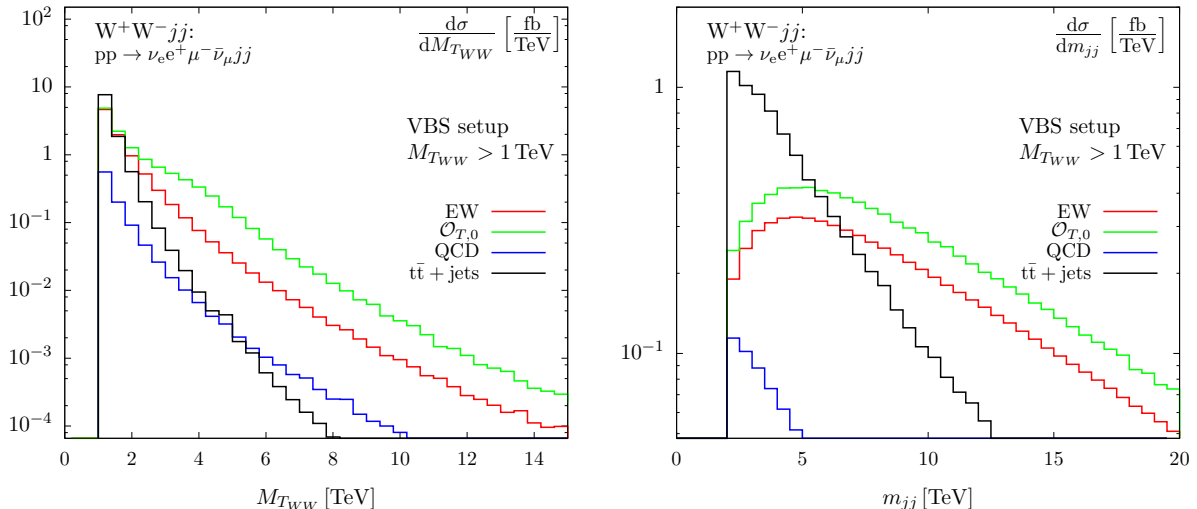


Figure 14: *Transverse mass of the  $W^+W^-$  system (l.h.s) and invariant mass of the tagging jets (r.h.s) in the framework of the SM (red lines) and including the impact of the dimension-eight operator  $\mathcal{O}_{T,0}$  (green lines) with the form factor of Eq. (23). Also shown are the the QCD-induced (blue lines), and the top-quark induced (black lines) background contributions. The selection cuts of Eqs. (11)–(14) and Eqs. (31)–(33) are imposed in each case.*

induced background contributions leaving us with an advantageous  $S/B$  ratio due to the dominance of the VBS signal in the remaining regions of phase space.

In analogy to the  $W^+W^+jj$  and  $ZZjj$  channels discussed previously, also in the  $W^+W^-jj$  case new-physics effects due to higher-dimensional operators are most pronounced at high scales. Fig. 14 shows the impact of the dimension-eight operator  $\mathcal{O}_{T,0}$ , again with a coefficient of  $f_{T,0}/\Lambda^4 = 0.1/\text{TeV}^4$ , supplied by the form factor of Eq. (23) with  $\Lambda_F = 4.7$  TeV, on the transverse-mass distribution of the  $W^+W^-$  system compared to the SM prediction. From the high-energy behavior of this observable we infer that the selection cut of Eq. (33) can efficiently improve the relative impact of the dimension-eight operator on the SM event rate. Indeed, applying this extra cut results in  $\sigma_{\text{SM}}^{\text{cut}} = 3.59$  fb and  $\sigma_{\text{EFT}}^{\text{cut}} = 4.80$  fb, to be compared to the respective results of  $\sigma_{\text{SM}} = 58.27$  fb and  $\sigma_{\text{EFT}} = 59.49$  fb before the cut of Eq. (33). While the remaining fraction of QCD background does not change much with  $M_{TWW}$ , the  $t\bar{t}$  (+jets) backgrounds fall precipitously with increasing  $W^+W^-$  transverse mass. This is caused by the high  $p_T$  of the top quarks which is needed to give the  $W$  bosons sufficient transverse mass and concomitant high  $p_T$ . The higher top-quark transverse momentum results, however, in harder bottom quarks, which increasingly fail the central jet veto cut of  $p_{T,b} < 50$  GeV. One finds, therefore, that the interesting very high transverse mass region has a rather small top-pair background and, thus, is particularly well suited for restricting anomalous quartic couplings at an FCC.

VBS channel	$\sigma_S$ [fb]	$\sigma_B$ [fb]	$S/B$	$S/\sqrt{B}$	$S/\sqrt{S+B}$
$W^+W^+jj$	0.48	0.04	12	416	115
$W^+Zjj$	0.047	0.008	5.9	91	35
$ZZjj$	0.11	0.008	13.7	213	56
$W^+W^-jj$	3.59	4.62	0.78	289	217

Table 2: Cross sections and different signal-background ratios for various VBS processes in the framework of the SM after the optimized cuts of Secs. 4.1–4.4 are imposed. Decays of the weak bosons into a specific leptonic final state are included as detailed in the text. In each case  $S$  denotes the number of events for the  $EW VVjj$  production mode, while  $B$  includes the number of background events due to the respective QCD  $VVjj$  channels and (in the  $W^+W^-jj$  case) top-induced production modes. An integrated luminosity of  $30 \text{ ab}^{-1}$  is assumed. Statistical errors are at the permille level in each case.

VBS channel	$\sigma_S$ [fb]	$\sigma_B$ [fb]	$S/B$	$S/\sqrt{B}$	$S/\sqrt{S+B}$
$W^+W^+jj$	0.66	0.52	1.27	159	105
$W^+Zjj$	0.061	0.055	1.11	45	31
$ZZjj$	0.22	0.12	1.83	110	65
$W^+W^-jj$	4.8	8.2	0.58	290	231

Table 3: Cross sections and different signal-background ratios for various VBS processes in the framework of the SM and including the impact of the dimension-eight operator  $\mathcal{O}_{T,0}$  with  $f_{T,0}/\Lambda^4 = 0.1/\text{TeV}^4$  and the form factor of Eq. (23) after the optimized cuts of Secs. 4.1–4.4 are imposed. Decays of the weak bosons into a specific leptonic final state are included as detailed in the text. In each case  $S$  denotes the number of events in the EFT scenario, while  $B$  includes the number of background events due to the respective SM  $EW$  and QCD  $VVjj$  channels as well as (in the  $W^+W^-jj$  case) top-induced production modes. An integrated luminosity of  $30 \text{ ab}^{-1}$  is assumed. Statistical errors are at the permille level in each case.

## 5 Summary and conclusions

In this article, we provided a review of VBS processes at a future 100 TeV hadron collider. We discussed how cuts tailored to specific final states can be used to efficiently suppress QCD and top-quark induced background contributions that exhibit entirely different kinematic properties than the signal processes of interest. In order to generically explore the capability of an FCC to identify signatures of new physics in the weak gauge boson sector, we provided representative results obtained in an EFT approach. While they hardly affect SM results at low scales, the considered BSM contributions have particular impact in the high-energy regime, significantly modifying the tails of transverse-momentum and invariant-mass distributions. These kinematic regimes are difficult to access at the LHC that is currently limited to a collider energy of 13 TeV. The possibility of a future 100 TeV hadron collider thus represents entirely new means for exploring new physics in the weak sector.

In Tabs. 2 and 3 we summarise signal and background cross sections for all discussed production modes within the optimized selection cuts we devised. For a representative integrated luminosity of  $30 \text{ ab}^{-1}$  we also list various ratios of signal and background event numbers. We first consider the SM EW  $VVjj$  production modes as signal and the respective QCD  $VVjj$  as well as, in the  $W^+W^-jj$  case, top-induced production modes as background. When we consider the EFT prediction as signal the sum of EW and QCD induced production cross sections is taken as background. In the latter case we restrict ourselves to the scenario with a non-vanishing dimension-eight operator  $\mathcal{O}_{T,0}$  which has the largest impact on the considered observables.

Starting from Tab. 3 one can perform a very rough extrapolation to smaller Wilson coefficients of  $\mathcal{O}_{T,0}$ : differential cross sections at high scales, for fixed form factor, scale like the square of the Wilson coefficient. The significances in the last column of Tab. 3 then suggest an FCC reach of at least  $0.01 \text{ TeV}^{-4}$  for the  $\mathcal{O}_{T,0}$  coefficient. This estimate is conservative since higher form factor scales are allowed for smaller anomalous quartic gauge couplings (aQGCs) and, also, more stringent cuts, focusing on even higher  $m_{VV}$  regions, will improve sensitivity. Decay distributions of the  $W$  and  $Z$  bosons can be used to improve sensitivity and to distinguish different dimension 8 operators. Finally, for the very hard weak bosons in the sensitive region of phase space, the analysis of hadronic  $V = W, Z$  decays with highly boosted  $V \rightarrow q\bar{q}$  jets will enhance sensitivity even further. Similar improvements are expected for other operators describing aQGCs. A realistic sensitivity estimate to aQGCs at an FCC needs to take these improvements into account and, thus, would go significantly beyond the scope of the present analysis.

## Acknowledgements

We are grateful for valuable discussions to Matthias Kesenheimer. The work of B. J. and L. S. has been supported in part by the Institutional Strategy of the University of Tübingen (DFG, ZUK 63), and in part by the German Federal Ministry for Education and Research (BMBF) under grant number 05H15VTCAA. The work of M. W. was supported by the DFG under Grant No. WO 1900/2 and by the BMBF under grant number 05H15PACC1. The work of D. Z. was supported by the BMBF under grant number 05H15VKCCA. The authors acknowledge support by the state of Baden-Württemberg through bwHPC and the German Research Foundation (DFG) through grant no INST 39/963-1 FUGG.

## References

- [1] G. Aad *et al.* [ATLAS Collaboration], "*Observation of a new particle in the search for the Standard Model Higgs boson with the ATLAS detector at the LHC*", Phys. Lett. B **716** (2012) 1 [arXiv:1207.7214 [hep-ex]].
- [2] S. Chatrchyan *et al.* [CMS Collaboration], "*Observation of a new boson at a mass of 125 GeV with the CMS experiment at the LHC*", Phys. Lett. B **716** (2012) 30 [arXiv:1207.7235 [hep-ex]].



- [3] M. J. Dolan, C. Englert and M. Spannowsky, “*Higgs self-coupling measurements at the LHC*”, JHEP **1210** (2012) 112 [arXiv:1206.5001 [hep-ph]].
- [4] M. J. Dolan, C. Englert, N. Greiner, K. Nordstrom and M. Spannowsky, “*hhjj production at the LHC*”, Eur. Phys. J. C **75** (2015) no.8, 387 [arXiv:1506.08008 [hep-ph]].
- [5] J. Baglio, A. Djouadi and J. Quevillon, “*Prospects for Higgs physics at energies up to 100 TeV*”, Rept. Prog. Phys. **79** (2016) 116201 [arXiv:1511.07853 [hep-ph]].
- [6] J. Baglio, A. Djouadi, R. Gröber, M. M. Mühlleitner, J. Quevillon and M. Spira, “*The measurement of the Higgs self-coupling at the LHC: theoretical status*”, JHEP **1304** (2013) 151 [arXiv:1212.5581 [hep-ph]].
- [7] T. Plehn and M. Rauch, “*The quartic higgs coupling at hadron colliders*”, Phys. Rev. D **72** (2005) 053008 [hep-ph/0507321].
- [8] A. Djouadi, W. Kilian, M. Mühlleitner and P. M. Zerwas, “*Production of neutral Higgs boson pairs at LHC*”, Eur. Phys. J. C **10** (1999) 45 [hep-ph/9904287].
- [9] U. Baur, T. Plehn and D. L. Rainwater, “*Determining the Higgs boson selfcoupling at hadron colliders*”, Phys. Rev. D **67** (2003) 033003 [hep-ph/0211224].
- [10] M. J. Duncan, G. L. Kane and W. W. Repko, “*WW Physics at Future Colliders*”, Nucl. Phys. B **272** (1986) 517.
- [11] J. Bagger, V. D. Barger, K. M. Cheung, J. F. Gunion, T. Han, G. A. Ladinsky, R. Rosenfeld and C.-P. Yuan, “*CERN LHC analysis of the strongly interacting WW system: Gold plated modes*”, Phys. Rev. D **52** (1995) 3878 [hep-ph/9504426].
- [12] J. M. Butterworth, B. E. Cox and J. R. Forshaw, “*WW scattering at the CERN LHC*”, Phys. Rev. D **65** (2002) 096014 [hep-ph/0201098].
- [13] G. Aad *et al.* [ATLAS Collaboration], “*Evidence for Electroweak Production of  $W^\pm W^\pm jj$  in  $pp$  Collisions at  $\sqrt{s} = 8$  TeV with the ATLAS Detector*”, Phys. Rev. Lett. **113** (2014) no.14, 141803 [arXiv:1405.6241 [hep-ex]].
- [14] V. Khachatryan *et al.* [CMS Collaboration], “*Study of vector boson scattering and search for new physics in events with two same-sign leptons and two jets*”, Phys. Rev. Lett. **114** (2015) no.5, 051801 [arXiv:1410.6315 [hep-ex]].
- [15] M. L. Mangano *et al.*, “*Physics at a 100 TeV pp collider: Standard Model processes*”, arXiv:1607.01831 [hep-ph].
- [16] D. Goncalves, T. Plehn and J. M. Thompson, “*Weak Boson Fusion at 100 TeV*”, arXiv:1702.05098 [hep-ph].
- [17] K. Arnold *et al.*, “*VBFNLO: A Parton level Monte Carlo for processes with electroweak bosons*”, Comput. Phys. Commun. **180** (2009) 1661 [arXiv:0811.4559 [hep-ph]].

- [18] M. Czakon, C. G. Papadopoulos and M. Worek, "Polarizing the Dipoles", JHEP **0908** (2009) 085 [arXiv:0905.0883 [hep-ph]].
- [19] A. Cafarella, C. G. Papadopoulos and M. Worek, "HELAC-PHEGAS: A Generator for all parton level processes", Comput. Phys. Commun. **180** (2009) 1941 [arXiv:0710.2427 [hep-ph]].
- [20] A. Kanaki and C. G. Papadopoulos, "HELAC: A Package to compute electroweak helicity amplitudes", Comput. Phys. Commun. **132** (2000) 306 [hep-ph/0002082].
- [21] C. G. Papadopoulos and M. Worek, "Multi-parton cross sections at hadron colliders", Eur. Phys. J. C **50** (2007) 843 [hep-ph/0512150].
- [22] G. Bevilacqua, M. Czakon, M. V. Garzelli, A. van Hameren, A. Kardos, C. G. Papadopoulos, R. Pittau and M. Worek, "HELAC-NLO", Comput. Phys. Commun. **184** (2013) 986 [arXiv:1110.1499 [hep-ph]].
- [23] C. G. Papadopoulos, "PHEGAS: A Phase space generator for automatic cross-section computation", Comput. Phys. Commun. **137** (2001) 247 [hep-ph/0007335].
- [24] A. van Hameren, "PARNI for importance sampling and density estimation", Acta Phys. Polon. B **40** (2009) 259 [arXiv:0710.2448 [hep-ph]].
- [25] A. van Hameren, "KALEU: A General-Purpose Parton-Level Phase Space Generator", [arXiv:1003.4953 [hep-ph]].
- [26] L. A. Harland-Lang, A. D. Martin, P. Motylinski and R. S. Thorne, "Parton distributions in the LHC era: MMHT 2014 PDFs", Eur. Phys. J. C **75** (2015) no.5, 204 [arXiv:1412.3989 [hep-ph]].
- [27] A. Buckley, Ferrando, S. Lloyd, K. Nordström, B. Page, M. Rufenacht, M. Schönherr and G. Watt, "LHAPDF6: parton density access in the LHC precision era", Eur. Phys. J. C **75** (2015) 132 [arXiv:1412.7420 [hep-ph]].
- [28] M. Cacciari, G. P. Salam and G. Soyez, "The Anti- $k(t)$  jet clustering algorithm", JHEP **0804** (2008) 063 [arXiv:0802.1189 [hep-ph]].
- [29] M. Rauch, "Vector-Boson Fusion and Vector-Boson Scattering", arXiv:1610.08420 [hep-ph].
- [30] K. Hagiwara, S. Ishihara, R. Szalapski and D. Zeppenfeld, "Low-energy effects of new interactions in the electroweak boson sector", Phys. Rev. D **48** (1993) 2182.
- [31] C. Degrande, N. Greiner, W. Kilian, O. Mattelaer, H. Mebane, T. Stelzer, S. Willenbrock, C. Zhang, "Effective Field Theory: A Modern Approach to Anomalous Couplings", Annals Phys. **335** (2013) 21. [arXiv:1205.4231 [hep-ph]].
- [32] O. J. P. Eboli, M. C. Gonzalez-Garcia and J. K. Mizukoshi, " $pp \rightarrow jje^\pm\mu^\pm\nu\nu$  and  $jje^\pm\mu^\mp\nu\nu$  at  $\mathcal{O}(\alpha_{em}^6)$  and  $\mathcal{O}(\alpha_{em}^4\alpha_s^2)$  for the study of the quartic electroweak gauge boson vertex at CERN LHC", Phys. Rev. D **74** (2006) 073005 [hep-ph/0606118].

- [33] B. Jäger and G. Zanderighi, "NLO corrections to electroweak and QCD production of  $W^+W^+$  plus two jets in the POWHEGBOX", JHEP **1111** (2011) 055 [arXiv:1108.0864 [hep-ph]].
- [34] B. Feigl, diploma thesis, Karlsruhe Institute of Technology (2010); O. Schlimpert, diploma thesis, Karlsruhe Institute of Technology (2013).
- [35] <https://www.itp.kit.edu/vbfnlo/wiki/doku.php?id=download:form-factor>
- [36] C. Englert, B. Jäger, M. Worek and D. Zeppenfeld, "Observing Strongly Interacting Vector Boson Systems at the CERN Large Hadron Collider", Phys. Rev. D **80** (2009) 035027 [arXiv:0810.4861 [hep-ph]].
- [37] G. Bevilacqua, M. Czakon, A. van Hameren, C. G. Papadopoulos and M. Worek, "Complete off-shell effects in top quark pair hadroproduction with leptonic decay at next-to-leading order", JHEP **1102** (2011) 083 [arXiv:1012.4230 [hep-ph]].
- [38] G. Bevilacqua, H. B. Hartanto, M. Kraus and M. Worek, "Top Quark Pair Production in Association with a Jet with Next-to-Leading-Order QCD Off-Shell Effects at the Large Hadron Collider", Phys. Rev. Lett. **116** (2016) no.5, 052003 [arXiv:1509.09242 [hep-ph]].
- [39] G. Bevilacqua, H. B. Hartanto, M. Kraus and M. Worek, "Off-shell Top Quarks with One Jet at the LHC: A comprehensive analysis at NLO QCD", JHEP **1611** (2016) 098 [arXiv:1609.01659 [hep-ph]].
- [40] C. Weiser, "A combined secondary vertex based B-tagging algorithm in CMS", CERN-CMS-NOTE-2006-014.
- [41] D. L. Rainwater and D. Zeppenfeld, "Observing  $H \rightarrow W^*W^* \rightarrow e^\pm\mu^\mp \cancel{p}_T$  in weak boson fusion with dual forward jet tagging at the CERN LHC", Phys. Rev. D **60** (1999) 113004 Erratum: [Phys. Rev. D **61** (2000) 099901] [hep-ph/9906218].
- [42] N. Kauer, T. Plehn, D. L. Rainwater and D. Zeppenfeld, " $H \rightarrow W^+W^-$  as the discovery mode for a light Higgs boson", Phys. Lett. B **503** (2001) 113 [hep-ph/0012351].
- [43] T. Figy, V. Hankele and D. Zeppenfeld, "Next-to-leading order QCD corrections to Higgs plus three jet production in vector-boson fusion", JHEP **0802** (2008) 076 [arXiv:0710.5621 [hep-ph]].
- [44] F. Campanario, T. M. Figy, S. Plätzer and M. Sjö Dahl, "Electroweak Higgs Boson Plus Three Jet Production at Next-to-Leading-Order QCD", Phys. Rev. Lett. **111** (2013) no.21, 211802 [arXiv:1308.2932 [hep-ph]].
- [45] B. Jäger, F. Schissler and D. Zeppenfeld, "Parton-shower effects on Higgs boson production via vector-boson fusion in association with three jets", JHEP **1407** (2014) 125 [arXiv:1405.6950 [hep-ph]].